Combustion and Flame 193 (2018) 170–176

Contents lists available at ScienceDirect

Combustion and Flame

journal homepage: www.elsevier.com/locate/combustflame

Brief Communications

Molecular conformational effects in H + *n*-heptane reaction rate calculations

Rasoul Nasiri[a,b,*], Kai H. Luo[a]

[a] Department of Mechanical Engineering, University College London, Torrington Place, London WC1E 7JE, UK
[b] Gas Purification Technology Group, Gas Research Division, Research Institute of Petroleum Industry (RIPI), P. O. Box 14665-137, Tehran, Iran

ARTICLE INFO

Article history:
Received 22 September 2017
Revised 31 October 2017
Accepted 8 March 2018

Keywords:
Conformational changes
Multi-pathway reactions
Reaction rate coefficients
Multi-structural statistical thermodynamics theory
Transition state theory

ABSTRACT

Accurate fuel combustion modelling is a matter of immense importance to design clean combustors and reduce greenhouse gas emissions and pollutants. In this Brief Communication, we present the effects of internal dynamics of one *n*-heptane molecule which are controlling chemical kinetics of hydrogen abstraction reactions through multi-pathway reaction dynamics. It is established that the slope of Arrhenius plots dramatically changes in comparison with the harmonic single static pathway approach in the temperature range of 200–3000 K. We apply a combination of the multiple conformation statistical thermodynamic approach and variational transition-state theory (VTST) to obtain dynamic multi-path rate coefficients ($k^{MP\text{-}T\text{-}VTST}$ and $k^{MP\text{-}LH\text{-}VTST}$). Compared with single-path VTST ($k^{SP\text{-}H\text{-}VTST}$) results, the thermal reaction rate coefficients obtained from our MP-VTST calculations differ considerably due to the fact that tunnelling and cross-conformational effects in the reactions, and the anharmonic and quasi-harmonic contributions in multiple conformer molecules cannot be ignored or simplified.

1. Introduction

Numerous experimental, theoretical and computational efforts have been focused on the pyrolysis reactions of alkanes for many decades [1–5]. Heptane is one of the most important *n*-alkane molecules that is found not only in petrol but also jet fuels for combustion engines. One of the key steps in the decomposition and combustion of *n*-heptane is the hydrogen abstraction reaction by atomic hydrogen and alkyl radicals [1,5] through the five main channels:

$$CH_3(CH_2)_5CH_3 + {}^{\bullet}H \rightarrow CH_3(CH_2)_5{}^{\bullet}CH_2 + H_2 \quad (C1)$$

$$CH_3(CH_2)_5CH_3 + {}^{\bullet}CH_3 \rightarrow CH_3(CH_2)_5{}^{\bullet}CH_2 + CH_4 \quad (C2)$$

$$CH_3(CH_2)_5CH_3 + {}^{\bullet}C_2H_5 \rightarrow CH_3(CH_2)_5{}^{\bullet}CH_2 + C_2H_6 \quad (C3)$$

$$CH_3(CH_2)_5CH_3 + {}^{\bullet}C_3H_7 \rightarrow CH_3(CH_2)_5{}^{\bullet}CH_2 + C_3H_8 \quad (C4)$$

$$CH_3(CH_2)_5CH_3 + {}^{\bullet}C_4H_9 \rightarrow CH_3(CH_2)_5{}^{\bullet}CH_2 + C_4H_{10} \quad (C5)$$

H_2 has been recognised experimentally and computationally as a major product in the pyrolysis of *n*-heptane [5]. The current work aims to provide new insights into chemical dynamics of hydrogen abstraction reactions taking place in the first channel which is split into the following channels;

$$CH_3(CH_2)_5CH_3 + {}^{\bullet}H \rightarrow CH_3(CH_2)_5{}^{\bullet}CH_2 + H_2 \quad (R1)$$

$$CH_3(CH_2)_4CH_2CH_3 + {}^{\bullet}H \rightarrow CH_3(CH_2)_4{}^{\bullet}CHCH_3 + H_2 \quad (R2)$$

$$CH_3(CH_2)_3CH_2CH_2CH_3 + {}^{\bullet}H \rightarrow CH_3(CH_2)_3{}^{\bullet}CHCH_2CH_3 + H_2 \quad (R3)$$

$$CH_3(CH_2)_2CH_2CH_2CH_2CH_3 + {}^{\bullet}H \rightarrow CH_3(CH_2)_2{}^{\bullet}CHCH_2CH_2CH_3 + H_2 \quad (R4)$$

Held *et al.* [6] pointed out the importance of including these four channels in the study of the mechanisms for *n*-heptane oxidation, as well as the relevance of knowing the proportions of each of these four radicals since they lead to different β-scission products. Indeed these radicals have been involved in low temperature autoignition chemistry [7] and influenced the intermediate temperature heat release (ITHR) in modern combustion engines [8] as well as cool flame chemistry [9]. These four H atom abstraction reactions have been considered as main channels of fuel consumption. A semi-empirical kinetic model was also validated using flow and stirred reactor experiments for these reactions [6].

* Corresponding author.
E-mail addresses: r.nasiri@ucl.ac.uk, nasiri1355@gmail.com (R. Nasiri).

https://doi.org/10.1016/j.combustflame.2018.03.010

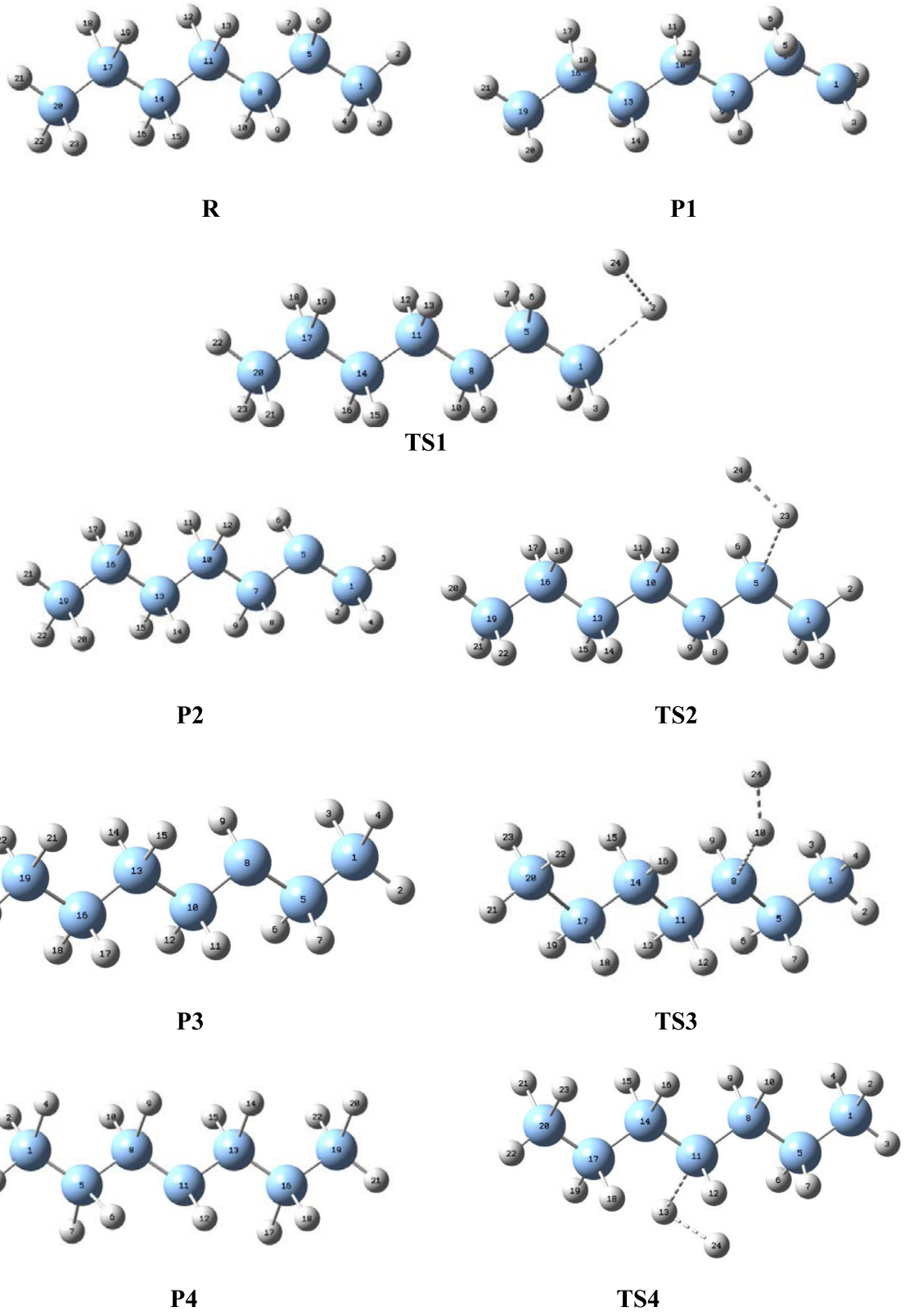

Fig. 1. ωB97X-D/cc-pVTZ optimised lowest-energy structures of the *n*-heptane (R), four heptyl radicals (P1, P2, P3 and P4) and transition states (TS1, TS2, TS3 and TS4) of the reactions of R1–R4.

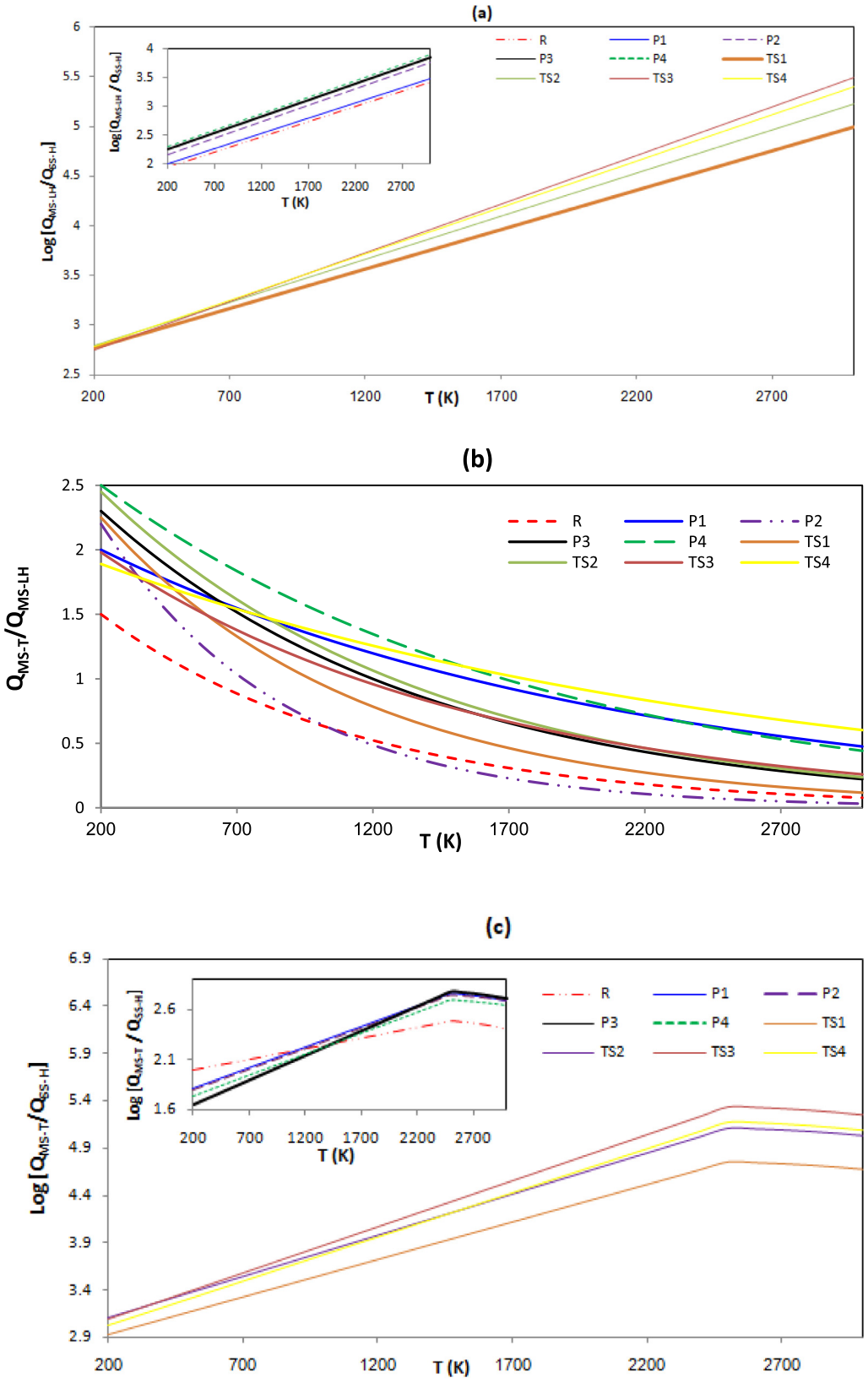

Fig. 2. The ratios of partition functions for all species in this study versus temperature in the gas phase: $Q_{MS\text{-}LH}/Q_{SS\text{-}H}$, (b) $Q_{MS\text{-}T}/Q_{MS\text{-}LH}$, and (c) $Q_{MS\text{-}T}/Q_{SS\text{-}H}$.

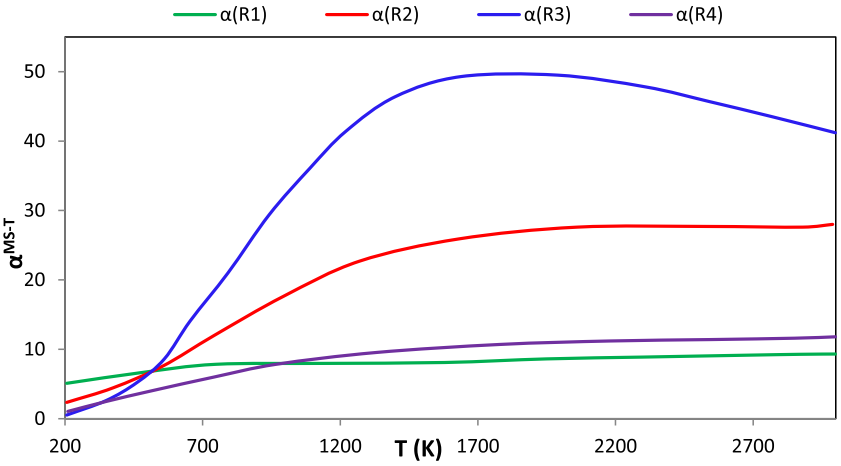

Fig. 3. Variations with temperature of α^{MS-T} calculated for the reactions of R1–R4 at CCSD(T)/cc-pVTZ//ωB97X-D/cc-pVTZ level of theory in the gas phase.

Table 1
The transmission coefficients of γ_1, $<\gamma>_7$ and $<\gamma>$ for reactions R1–R4 of hydrogen abstraction of *n*-heptane. The coefficients were computed using the CCSD(T)/cc-pVTZ//ωB97X-D/cc-pVTZ chemistry model.

	Reactions			
T (K)	R1	R2	R3	R4
	γ_1 (MS-VTST)			
200	0.98	0.93	0.97	0.97
500	0.98	0.95	0.95	0.98
1000	0.98	0.96	0.93	0.99
2000	0.99	0.96	0.93	0.99
3000	0.99	0.97	0.93	0.99
	$<\gamma>_7$ (MP-VTST)			
200	2.99	1.96	0.96	1.48
500	2.58	1.25	0.93	1.09
1000	1.43	1.01	0.93	1.02
2000	1.20	0.99	0.92	0.98
3000	1.08	0.93	0.90	0.95
	$<\gamma>$ (MP-VTST)			
200	2.93	1.97	0.98	1.60
500	2.81	1.92	0.97	1.49
1000	2.67	1.75	0.95	1.41
2000	2.39	1.52	0.94	1.35
3000	2.25	1.42	0.93	1.29

It was assumed that a sequence of reactions of abstraction and decomposition as an overall H-abstraction reaction implies some difficulties in the determination of chemical kinetic parameters such as activation energy of each step experimentally [6]. Perhaps, the best estimate is a computational study carried out by Han and co-workers [1], although these authors introduce some approximations which may affect the accuracy of the calculated thermal rate coefficients. For instance, they considered the most stable structure for each reactant, transition states and products involved in reactions R1–R3 but conformational changes in these structures will lead to multiple pathways in all four channels of R1–R4.

The objective of this work is to study reactions R1–R4 taking into account all the possible conformers relevant to the H atom abstraction chemical reaction dynamics. The electronic structure method is applied in combination with the multistructural statistical thermodynamic method [10–14] to simulate the hydrogen abstraction reaction dynamics in four sites of *n*-heptane. The results of multipath variational transition state theory (MP-VTST) are analysed with the emphasis on the key role of conformational changes while *quantum tunnelling* and *torsional anharmonicity* effects are also being taken into account to reveal the underlying chemical dynamics mechanisms responsible for one of the most important steps in the pyrolysis of *n*-heptane (see Supplementary Materials for the details of Theory and Computational Meth-

Table 2
The harmonic SP-H-VTST, quasi-harmonic MP-LH-VTST and anharmonic MP-T-VTST reaction rate parameters (A, n, E_a and T_0) for the reactions of R1–R4 and overall reaction. Units are as follows: cm^3 $molecule^{-1}$ s^{-1}, kcal mol^{-1}, K.

	Reactions				
Parameters	R1	R2	R3	R4	R1 + R2 + R3 + R4
	SP-H-VTST				
A	7.00E-13	1.00E-12	3.50E-13	9.00E-13	8.00E-12
n	1.55	1.85	2.7	2.35	1.85
E_a	15.9	15	16	15.3	15
T_0	280	85	150	80	120
	MP-LH-VTST				
A	8E-16	5E-16	7E-16	9E-17	9E-16
n	5.4	6	7.2	7.2	7.2
E_a	6	6.8	5.5	4.9	7.15
T_0	200	400	210	170	300
	MP-T-VTST				
A	1.01E-13	1.05E-13	1E-13	7.5E-14	1.35E-13
n	2.21	2.18	2.65	2.85	2.99
E_a	6.9	4.4	4.8	4.95	4.8
T_0	100	400	220	200	150

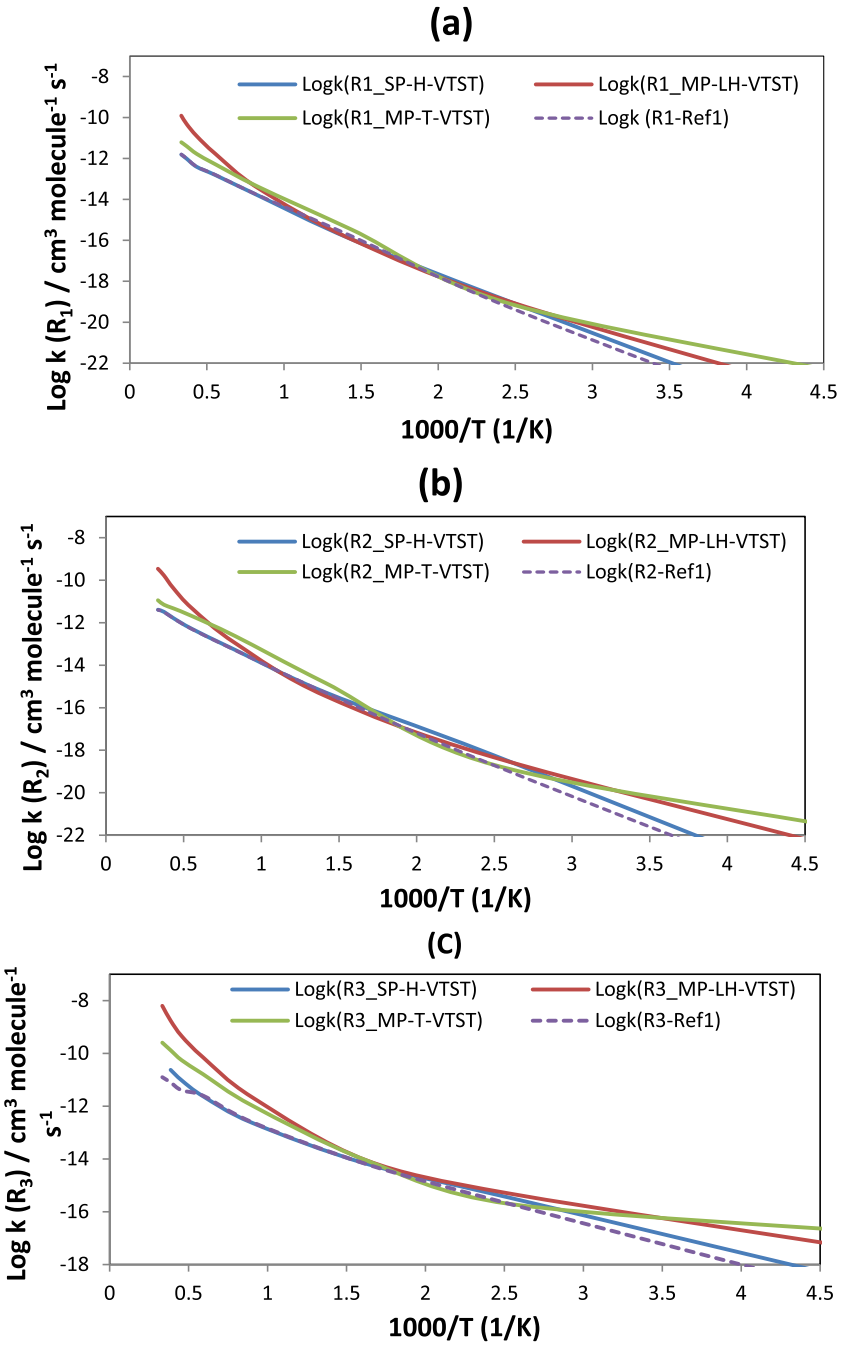

Fig. 4. Variations with temperature of rate coefficients (solid lines) computed at CCSD(T)/cc-pVTZ//ωB97X-D/cc-pVTZ level of theory in the gas phase using partition functions of $Q_{SS\text{-}H}$ ($k^{SP\text{-}H\text{-}VTST}$), $Q_{MS\text{-}LH}$ ($k^{MP\text{-}LH\text{-}VTST}$) and $Q_{MS\text{-}T}$ ($k^{MP\text{-}T\text{-}VTST}$) for H-abstraction reactions of (a) R1, (b) R2, and (c) R3. The theoretical work reported in [1] (dash lines) with CCSD(T)/6–311G(d,p)//B3LYP/6– 311G(d,p) is also plotted for comparison.

ods). The method presented in this study is rather general and can be applied to any mechanism involved in combustion of hydrocarbons and oxygenate compounds which have significant effects of multiple structures, multiple transition states, and multiple pathways.

2. Results and discussion

In order to compare the single- and multi-pathway H-abstraction reaction rate coefficients, we have first fully optimised all the conformers of *n*-heptane molecule, heptyl radicals and transition states of the reactions of R1–R4 using the ωB97X-D/cc-pVTZ chemistry model which has been established to provide accurate geometries and electronic energies close to those predicted by CCSD(T)/cc-pVTZ for *n*-alkanes [15]. The optimised global minimum geometries of *n*-heptane (hereafter denoted R), 1-helptyl (P1), 2-heptyl (P2), 3-heptyl (P3), 4-heptyl (P4) and transition states of the reactions (TS1, TS2, TS3 and TS4) are presented in Fig. 1.

We have then calculated three different partition functions $Q_{SS\text{-}H}$, $Q_{MS\text{-}LH}$ and $Q_{MS\text{-}T}$ for the reactants and transition states to determine $\alpha^{MS\text{-}LH}$ and $\alpha^{MS\text{-}T}$ factors which account for multiple structures and torsional anharmonicity effects (see Supplementary Materials). Numerous works have simplified these two effects in chemical reactions [1,16,17]. For example, in [1] authors estimated the pyrolysis reaction rate coefficients of *n*-heptane based

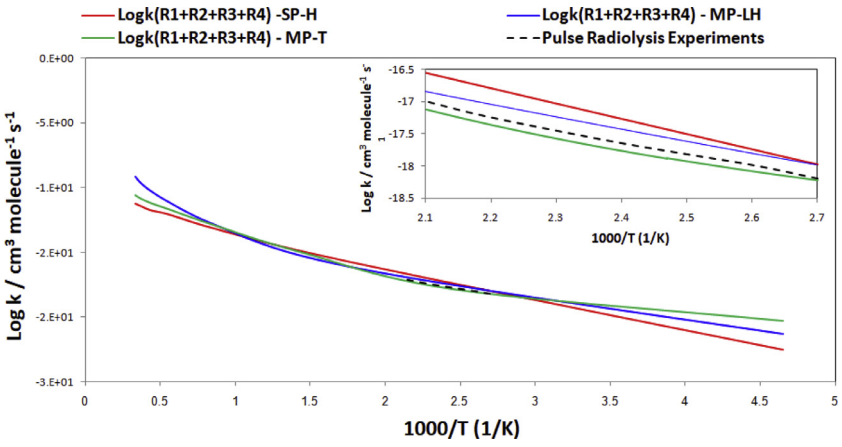

Fig. 5. Variations with temperature of overall rate coefficients (solid lines) computed using three partition functions of Q_{SS-H}, Q_{MS-LH} and Q_{MS-T}. The experimental data reported in [19] (dash lines) over the temperature range 363–463 K using the pulse radiolysis technique is also plotted for comparison.

on single structure harmonic (Q_{SS-H}) approximation considering only the lowest energy transition states and the most stable reactant and products. However, we have used a set of conformers of TS1, TS2, TS3, TS4, P1, P2, P3, P4 and R to consider the "local-harmonic multi-pathway" effect during the reaction pathways in each channel of R1–R4 to establish the large multiple structures effects on Q_{MS-LH} partition function. The ratios of Q_{MS-LH} per Q_{SS-H} for R molecule with 26 structures (all enantiomers have been excluded), P1 molecule with 31 structures and TS1 with 74 structures are 8.1×10^2, 9.1×10^2 and 4.0×10^4, respectively, at 2500 K (See Fig. 2a). In another study [17], the hindered rotors of *n*-propyl benzene molecule have been considered using one dimensional quasi-harmonic model (Q_{MS-QH}) to predict H-abstraction reaction rate coefficients in the *n*-alkyl side chain structures. As seen in Fig. 2b and c, the combined effect of multiple structures with torsional anharmonicities or "torsions in multi-structure" (Q_{MS-T}) is different from Q_{MS-LH} and far removed from Q_{SS-H}. Therefore, Fig. 2a–c illustrates the effect of multiple structures and torsional anharmonicity in the chemical species involved in the reactions of R1–R4. Since the ratios are very large for saddle point structures in comparison with the stationary ones, we provide the ratios for reactants and products in the inset of Fig. 2a and c. Figure 2a and b present the multiple structures quasi-harmonic and torsional anharmonic effects using respectively ratios of Q_{MS-LH}/Q_{SS-H} and Q_{MS-T}/Q_{MS-LH}. The combination of these two effects is given in Fig. 2c, where Q_{MS-T}/Q_{SS-H} is depicted as a function of temperature. These three figures also show that the contributions of multiple structures and the torsional potential anharmonicity increase at all temperatures up to 2500 K and then decrease at higher temperatures, respectively. Curves of Q_{MS-T}/Q_{MS-LH} do not follow the same trends as those of Fig. 2a and c. The ratios of Q_{MS-T}/Q_{SS-H} also show a decreasing trend after 2500 K. These inverse trends can be understood due to the fact that the contribution of torsional potential anharmonicities is less important than multiple structures effect when the temperature goes up. As the anharmonic/quasi-harmonic effects are different between the reactant/products and the transition states (e.g., total number of structures are not the same), we expect that the overall moment inertia of reactions effectively change.

The variations of the values of α^{MS-T} versus temperature are presented in Fig. 3. This figure shows that the α^{MS-T} factor passes through a maximum for reaction R3, whereas for the others, the lines increase monotonically with different slops. The α^{MS-T} factor for R3 is about 10 times larger than for R1. It is worth mentioning that the ratios of partition functions for TS3 are also larger than others in Fig. 2a and c. These findings confirm the importance of quasi-harmonic and anharmonic effects of multiple transition states TS3 in estimation of H-abstraction reaction rate coefficients.

The multi-structural statistical thermodynamics method and conventional TST do not include the quantum tunnelling and cross-conformational effects which are important in H-abstraction reactions. We calculate a combined effect of these correction terms known as "transmission coefficient" (γ) in the estimation of the canonical multi-path and multi-structural variational transition state theory (MP-VTST and MS-VTST) (see refs. [13,14] and SI for more details). The values of these correction terms are illustrated in Table 1 for reactions R1–R4 with one (γ_1), seven ($<\gamma>_7$) and all possible saddle points ($<\gamma>$). At 200 K, $<\gamma>$ and $<\gamma>_7$ values are close, confirming that this reaction is mainly proceded by using up to seven transition states. The deviation between $<\gamma>$ and $<\gamma>_7$ values becomes significant at high temperatures as one will deal with errors between 67% and 48% in the estimation of the rate coefficient of the R1 reaction when one and seven saddle points are taken into account in comparison with the case in which all possible saddle points have been considered. Note that besides these errors, others also arise from the variation of α^{MS-T} which is an anharmonic factor induced by multiple conformations and torsions in the local minima (see SI for more details). Therefore, one needs to distinguish these two different factors, γ and α^{MS-T}, in the estimation of the reaction rate coefficients.

The rate coefficients of $k^{SP-H-VTST}$, $k^{MP-LH-VTST}$ and $k^{MP-T-VTST}$ versus the temperature have been predicted for reactions R1–R3. These three rate coefficients which are shown in Fig. 4a–c present the contribution of each partition functions of Q_{SS-LH}, Q_{MS-LH} and Q_{MS-T} alongside the tunnelling and cross-conformational effects to the reactions R1–R3 (see Figures S1a–c in Supplementary Materials for the all reactions). While our SP-H-VTST rate coefficients have good agreement with computational results reported in [1] (see Fig. 4a), there are 3-4 order of magnitude difference between these results and our MP-LH-VTST and MP-T-VTST rate coefficients at high temperatures and especially at near room temperatures in which quantum tunnelling and cross-conformational effects are significant.

These rate coefficients are fitted with the following four-parameter expression which is an appropriate approximation for the endothermic reactions such as H-abstraction [18]. The plots which consider multi-pathways are curved rather than straight lines.

$$k = A\left(\frac{T+T_0}{300}\right)^n \times e^{-E_a(T+T_0)/R(T^2+T_0^2)} \quad (1)$$

where R is the gas constant. All fitting parameters (A, n, E_a, and T_0) are tabulated in Table 2.

In addition to a semi-empirical kinetic model and the flow/stirred reactor measurements [6], mentioned in the introduction, other experiments carried out by Fujisaki *et al.* [19] using pulse radiolysis of vapour water containing *n*-heptane over the temperature range of 363–463 K. They measured overall rate coefficients for the reaction R1 + R2 + R3 + R4. These total reaction rate coefficients are calculated from site-specific rate coefficients of k_{R1}, k_{R2}, k_{R3} and k_{R4} as their sum-up. As compared from the curves in Fig. 5, our MP-T-VTST and MP-LH-VTST results are in good agreement with the measured experimental values [19] over the temperature range 363–463 K. On the other hand, SP-H-VTST model could not reproduce these reliable and accurate thermal reaction rate coefficient values.

To conclude, the present theoretical and computational efforts quantify the effects of classical conformational and quantum cross-conformational in *n*-heptane conformers to accurately predict the H-abstraction reaction rate coefficients dynamically. The main findings in this study are that taking account of multi-pathway, torsional and tunnelling effects increases the rate coefficients for H + *n*-heptane reactions by 3-4 orders of magnitude compared to prior work in [1] where these factors were not included. This study has also provided more detailed information for chemical kinetics of pyrolysis reactions of *n*-heptane which are difficult to measure by experiments. Further investigations are on-going to fully understand how these correction terms affect other chemical reactions involved in the combustion processes.

Acknowledgments

This research is funded by the UK Engineering and Physical Sciences Research Council under the project “UK Consortium on Mesoscale Engineering Sciences (UKCOMES)” (grant no. EP/L00030X/1). The authors are grateful to Professor Truhlar for providing us with the Polyrate, MSTor and Gaussrate codes.

Supplementary materials

Supplementary material associated with this article can be found, in the online version, at doi:10.1016/j.combustflame.2018.03.010.

References

[1] J. Ding, L. Zhang, K. Han, Thermal rate constants of the pyrolysis of n-heptane, Combust. Flame 158 (2011) 2314–2324.
[2] H.H. Voge, G.M. Good, Thermal cracking of higher paraffins, J. Am. Chem. Soc. 71 (1949) 593–597.
[3] B.M. Fabuss, J.O. Smith, R.I. Lait, A.S. Borsanyi, C.N. Satterfield, Rapid thermal cracking of n-hexadecane at elevated pressures, Ind. Eng. Chem. Process Des. Dev. 1 (1962) 293.
[4] C. Song, W.C. Lai, H.H. Schobert, Condensed-phase pyrolysis of n-tetradecane at elevated pressures for long duration, product distribution and reaction mechanisms, Ind. Eng. Chem. Res. 33 (1994) 534–547.
[5] T. Yuan, L. Zhang, Z. Zhou, M. Xie, L. Ye, F. Qi, Pyrolysis of n-heptane: experimental and theoretical study, J. Phys. Chem. A 115 (2011) 1593–1601.
[6] T.J. Held, A.J. Marchese, F.L. Dryer, A semi-empirical reaction mechanism for n-heptane oxidation and pyrolysis, Combust. Sci. Technol. 123 (1997) 107–146.
[7] J. Zádor, C.A. Taatjes, R.X. Fernandes, Kinetics of elementary reactions in low-temperature autoignition chemistry, Prog. Energy Combust. Sci. 37 (2011) 371–421.
[8] D. Vuilleumier, D. Kozarac, M. Mehl, S. Saxena, W.J. Pitz, R.W. Dibble, J.-Y. Chen, S.M. Sarathy, Intermediate temperature heat release in an HCCI engine fuelled by ethanol/*n*-heptane mixtures: an experimental and modeling study, Combustion Flame 161 (2014) 680–695.
[9] Z. Wan, B. Chen, K. Moshammer, D.M. Popolan-Vaida, S. Sioud, V.S.B. Shankar, D. Vuilleumier, T. Tao, L. Ruwe, E. Bräuer, N. Hansen, P. Dagaut, K. Kohse-Höinghaus, M.A. Raji, S.M. Sarathy, *n*-Heptane cool flame chemistry: unraveling intermediate species measured in a stirred reactor and motored engine, Combust. Flame 187 (2018) 199–216.
[10] J. Zheng, T. Yu, E. Papajak, I.M. Alecu, S.L. Mielke, D.G. Truhlar, Practical methods for including torsional anharmonicity in thermochemical calculations on complex molecules: the internal-coordinate multi-structural approximation, Phys. Chem. Chem. Phys. 13 (2011) 10885.
[11] J. Zheng, D.G. Truhlar, Including torsional anharmonicity in canonical and microcanonical reaction path calculations, J. Chem. Theory Comput. 9 (2013) 2875–2881.
[12] T. Yu, J. Zheng, D.G. Truhlar, Multi-path variational transition state theory. Rate constant of the 1,4-hydrogen shift isomerization of the 2-cyclohexylethyl radical, J. Phys. Chem. A 116 (2012) 297–308.
[13] J. Zheng, D.G. Truhlar, Multi-path variational transition state theory for chemical reaction rates of complex polyatomic species: ethanol + OH reactions, Faraday Discuss. 157 (2012) 59–88 See also Discussion remarks on pages 113–115, 122, 125–129, 137, 139-140, 244, 245, 258, 265-266, 376, 388, 395, 478, 491-492, 494-495, and 500.
[14] J. Zheng, D.G. Truhlar, Quantum thermochemistry: multi-structural method with torsional anharmonicity based on a coupled torsional potential, J. Chem. Theory Comput. 9 (2013) 1356–1367.
[15] R. Nasiri, V.M. Gun'ko, S.S. Sazhin, The effects of internal molecular dynamics on the evaporation/condensation of *n*-dodecane, Theor. Chem. Acc. 134 (2015) 1–12.
[16] H. Tao, K.C. Lin, Kinetic barriers, rate constants and branching ratios for unimolecular reactions of methyl octanoate peroxy radicals: a computational study of a mid-sized biodiesel fuel surrogate, Combust. Flame 180 (2017) 148–157.
[17] R.K. Robinson, R.P. Lindstedt, A comparative ab initio study of hydrogen abstraction from *n*-propylbenzene, Combust. Flame 160 (2013) 2642–2653.
[18] P. Seal, G. Oyedepo, D.G. Truhlar, Kinetics of the hydrogen atom abstraction reactions from 1-butanol by hydroxyl radical: theory matches experiment and more, J. Phys. Chem. A 117 (2013) 275–282.
[19] N. Fujisaki, A. Ruf, T. Gäumann, Kinetic isotope effects for hydrogen abstractions from *n*-alkanes by hydrogen atoms in the gas phase, J. Chem. Phys. 80 (6) (1984) 2570–2577.